



Live-cell measurements of kinase activity in single cells using translocation reporters

Takamasa Kudo¹, Stevan Jeknić², Derek N Macklin² , Sajia Akhter², Jacob J Hughey^{2,3} , Sergi Regot^{2,3} & Markus W Covert^{1,2}

¹Department of Chemical and Systems Biology, Stanford University, Stanford, California, USA. ²Department of Bioengineering, Stanford University, Stanford, California, USA. ³Present addresses: Department of Biomedical Informatics, School of Medicine, Vanderbilt University, Nashville, Tennessee, USA (J.J.H.); Department of Molecular Biology and Genetics, School of Medicine, Johns Hopkins University, Baltimore, Maryland, USA (S.R.). Correspondence should be addressed to M.W.C. (mcovert@stanford.edu) or S.R. (sregot@jhmi.edu).

Published online 21 December 2017; doi:10.1038/nprot.2017.128

Although kinases are important regulators of many cellular processes, measuring their activity in live cells remains challenging. We have developed kinase translocation reporters (KTRs), which enable multiplexed measurements of the dynamics of kinase activity at a single-cell level. These KTRs are composed of an engineered construct in which a kinase substrate is fused to a bipartite nuclear localization signal (bNLS) and nuclear export signal (NES), as well as to a fluorescent protein for microscopy-based detection of its localization. The negative charge introduced by phosphorylation of the substrate is used to directly modulate nuclear import and export, thereby regulating the reporter's distribution between the cytoplasm and nucleus. The relative cytoplasmic versus nuclear fluorescence of the KTR construct (the C/N ratio) is used as a proxy for the kinase activity in living, single cells. Multiple KTRs can be studied in the same cell by fusing them to different fluorescent proteins. Here, we present a protocol to execute and analyze live-cell microscopy experiments using KTRs. We describe strategies for development of new KTRs and procedures for lentiviral expression of KTRs in a cell line of choice. Cells are then plated in a 96-well plate, from which multichannel fluorescent images are acquired with automated time-lapse microscopy. We provide detailed guidance for a computational analysis and parameterization pipeline. The entire procedure, from virus production to data analysis, can be completed in ~10 d.

INTRODUCTION

Protein kinases, the enzymes facilitating phosphate group transfer onto protein substrates, comprise one of the largest gene families in eukaryotes and are estimated to account for nearly 2% of all human genes¹. Protein phosphorylation regulates almost every cellular process, with one-third of human proteins predicted to be phosphorylated on at least one site². In particular, kinases are important regulators of signal transduction because of their ability to quickly and reversibly control protein functions. It is now known that cells can transmit information robustly through the dynamics of kinase activation^{3,4}. Environmental information such as stimulus type, intensity, or duration can be encoded into a specific temporal pattern of kinase activation and decoded as specific transcriptional and phenotypic cellular responses. The mechanism of this dynamics-dependent encoding and decoding has been challenging to investigate because of the large phenotypic heterogeneity present among isogenic cells. Each cell is exposed to a unique microenvironment, and the stochastic nature of biochemical reactions further creates differences in molecule copy number, signaling, and other cellular properties. In some cases, such stochasticity is used for collective cell decision making^{5–7}. Thus, to study the connection between signaling and cellular phenotypes^{8,9}, reporters to probe kinase activity dynamics at a single-cell level are desirable.

Here, we describe a technique to monitor kinase activity in a live-cell and single-cell manner. KTRs are genetically encoded fluorescent reporters that convert kinase activity into a nucleocytoplasmic shuttling event¹⁰. Localization changes are commonly mediated by phosphorylation in cells, and KTRs exploit this process to facilitate kinase reporter development. Briefly, a KTR is an

engineered construct in which a kinase substrate is fused to a bNLS and NES—either of which may be phosphorylatable—as well as to a fluorescent protein (Fig. 1). The negative charge of a phosphate group near the bNLS or NES can affect localization of the KTR, presumably by changing binding affinities of the KTR to the nuclear import and export machinery^{10–12}. As a result, import can be inhibited and/or export enhanced. Thus, the relative cytoplasmic versus nuclear fluorescence of the KTR construct (the C/N ratio), which intrinsically takes variability in KTR expression across cells into account, can serve as a proxy for kinase activity in living, single cells over time^{8,10,13,14}.

Advantages of KTR

Before KTRs, the most popular live, single-cell kinase reporters were based on Förster resonance energy transfer (FRET)¹⁵. One advantage of KTRs, as compared with the FRET-based kinase reporters, is the capacity to multiplex measurements in a single cell, as FRET-based reporters require two fluorescent proteins with very specific spectral properties. The FRET color requirement is, therefore, problematic not only for multiplexed measurements, but also for photobleaching and phototoxicity in some cases¹⁶. On the other hand, a fluorescent protein encoded within a KTR can be flexibly swapped. Moreover, multiplexing is relatively simple as long as different KTRs are fused to fluorescent proteins with minimal spectral overlap (Table 1); for example, three KTRs have been used together to determine the dynamics of ERK, JNK, and p38 simultaneously in a single cell¹⁰.

Another strength of KTRs is the relatively straightforward design process. The design or optimization of FRET-based

PROTOCOL

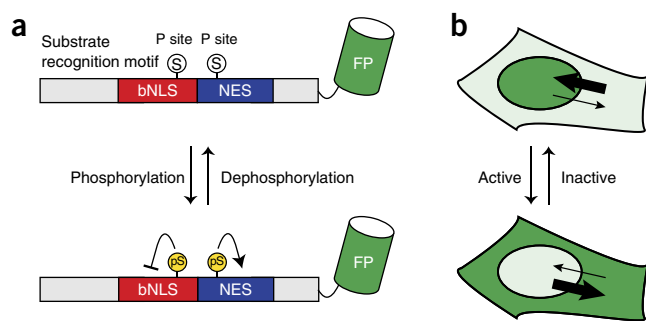


Figure 1 | Schematic representation of KTRs. **(a)** KTRs consist of a substrate recognition motif, phosphorylation sites (P sites) located near bNLS and NES sites, and a fluorescent protein (FP) domain. KTR phosphorylation suppresses bNLS activity and enhances NES activity, leading to cytoplasmic translocation of fluorescence. **(b)** Schematic representation of the subcellular distribution of the KTRs. When kinase activity is high, KTRs predominantly localize to the cytoplasm as a result of a decreased import rate and increased export rate.

reporters can be challenging, as FRET activity strongly depends on both the distance and the orientation of the donor and acceptor proteins, which are often difficult to predict. By contrast, the major determinants of the dynamic range of KTRs are the positions of phosphorylated residues and sequences of localization signals consisting of 10–20 aa, which are well characterized by previous studies^{17,18}. In addition, some evidence suggests that KTRs are able to capture deactivation dynamics better than the FRET-based reporters¹⁰. This is most likely because, once phosphorylated, FRET-based reporters may assume a tightly closed conformation that is not readily accessible to phosphatases. KTRs rapidly and continuously shuttle between nucleus and cytoplasm, and phosphorylation appears to affect only the flux of shuttling events. Therefore, it is likely that the accessibilities of KTRs to phosphatases and kinases are relatively robust to their phosphorylation status. As a result, slower dephosphorylation has been observed with the FRET-based JNK reporter than with the JNK KTR¹⁰.

Furthermore, the applicability of phosphomimetic and non-phosphorylatable amino acid substitution via simple mutagenesis provides another unique capacity of KTRs to estimate single, live-cell active kinase fractions. Substitution of the phosphorylation residue of serine or threonine (S/T) to glutamate (E) or alanine (A) can reproduce the localization of phosphorylated and unphosphorylated KTRs, respectively^{10,19}. Using these constructs, we can define the full dynamic range of a reporter from 0 to

100%. This is useful for reporter development and also enables parameterization of a mathematical model of kinase activation and deactivation based on KTR translocation¹⁰.

Limitations of KTR

One advantage of FRET-based reporters is that they can be used to measure kinase activities specific to subcellular compartments^{20–22}. By contrast, KTRs can monitor only global kinase activities that occur in the cytoplasm and/or nucleus¹⁰, and are, therefore, not suitable for studying kinases with locally regulated function. Moreover, kinase activity dynamics that occur during nuclear envelope breakdown cannot be measured with KTRs.

Next, although novel KTRs are relatively easy to develop, there are some challenging aspects of the process. First, we have found that KTRs often require more than one phosphorylation site in order to produce sufficient localization changes¹⁰. This adds complexity to the reporter development process. In addition, certain amino acid sequences near the phosphorylation sites can impact the efficiency of kinase recognition and KTR localization²³. This means that for some kinases, the KTR dynamic range might be suboptimal. Third, specificity is a very important consideration in developing both KTR and FRET-based reporters. This is because many kinases in nature are known to be promiscuous in terms of substrate. For example, most of the members of the AGC kinase family have a common recognition motif ‘RXRXX(pS/pT)’, but their substrates were shown to be recognized by different AGC kinases with a different affinity^{24,25}. Reporter specificity must, therefore, be assessed in order to interpret either KTR or FRET signals properly.

It is important to note that the cytoplasmic translocation of KTR is a relative measure of kinase activity. As each reporter has a unique sensitivity and dynamic range, the degree of translocation of different KTRs cannot be directly compared. For cases in which an antibody against the phosphorylated residue is available, a relationship between the phosphorylation status of the original substrate and the KTR translocation can be derived^{10,14}. Moreover, in the **Supplementary Methods**, we present a working example of how the absolute active and inactive JNK concentrations can be calculated by constructing a mathematical model with experimentally measured and literature parameters. However, the feasibility of this approach depends on the availability of molecular tools or published parameter values, as well as the dynamics exhibited by the reporter itself (see **Supplementary Methods** for more details).

Finally, KTR translocation can be influenced not only by kinase and phosphatase activity, but also by the nuclear export and import rates. Our own experiments suggest that the variability

TABLE 1 | Details of filters used to image fluorescent proteins.

Channel name	Excitation filter transmission (nm)	Emission filter transmission (nm)	Example fluorescent protein or stain
CFP	430 ± 24	470 ± 24	mCerulean3
YFP	500 ± 20	535 ± 30	mClover
TRITC	555 ± 25	605 ± 52	mRuby2
Far-red	645 ± 30	705 ± 72	iRFP670
Hoechst	350 ± 50	490 ± 20	Hoechst 33342

of these rates is negligible and large, consistent translocation of KTRs has been observed in many cell lines, including primary cells (**Supplementary Fig. 1**)¹⁰. However, it is certainly conceivable that the dependence of nuclear translocation rates on cell type or line might be another factor to consider in designing KTR experiments. The variability in import or export can be assessed in any given system by using phosphomimetic and nonphosphorylatable mutants, and can even be corrected by co-expressing these mutants¹⁰.

Level of expertise needed to implement the protocol

The experimental work described here requires some experience with molecular cloning; cell culture, including BSL-2 protocols for handling lentivirus; and live-cell microscopy.

For the computational pipeline, some experience with the Python programming language would facilitate using CellTK, but this is not strictly necessary, as parameter tuning and algorithm selection can be controlled by modifying a human-readable YAML file. Yet the primary aim of CellTK design is to provide flexibility and extensibility, which allow intermediate Python users to quickly try a number of algorithms to seek a suitable operation for their experiments and even add a function if needed. Further computing expertise would be required if parallel processing of image data in a cluster server is desired to reduce overall processing time.

The parameter estimation process for modeling absolute kinase concentration requires some knowledge of systems biology and/or mathematical modeling. The type of experiments required,

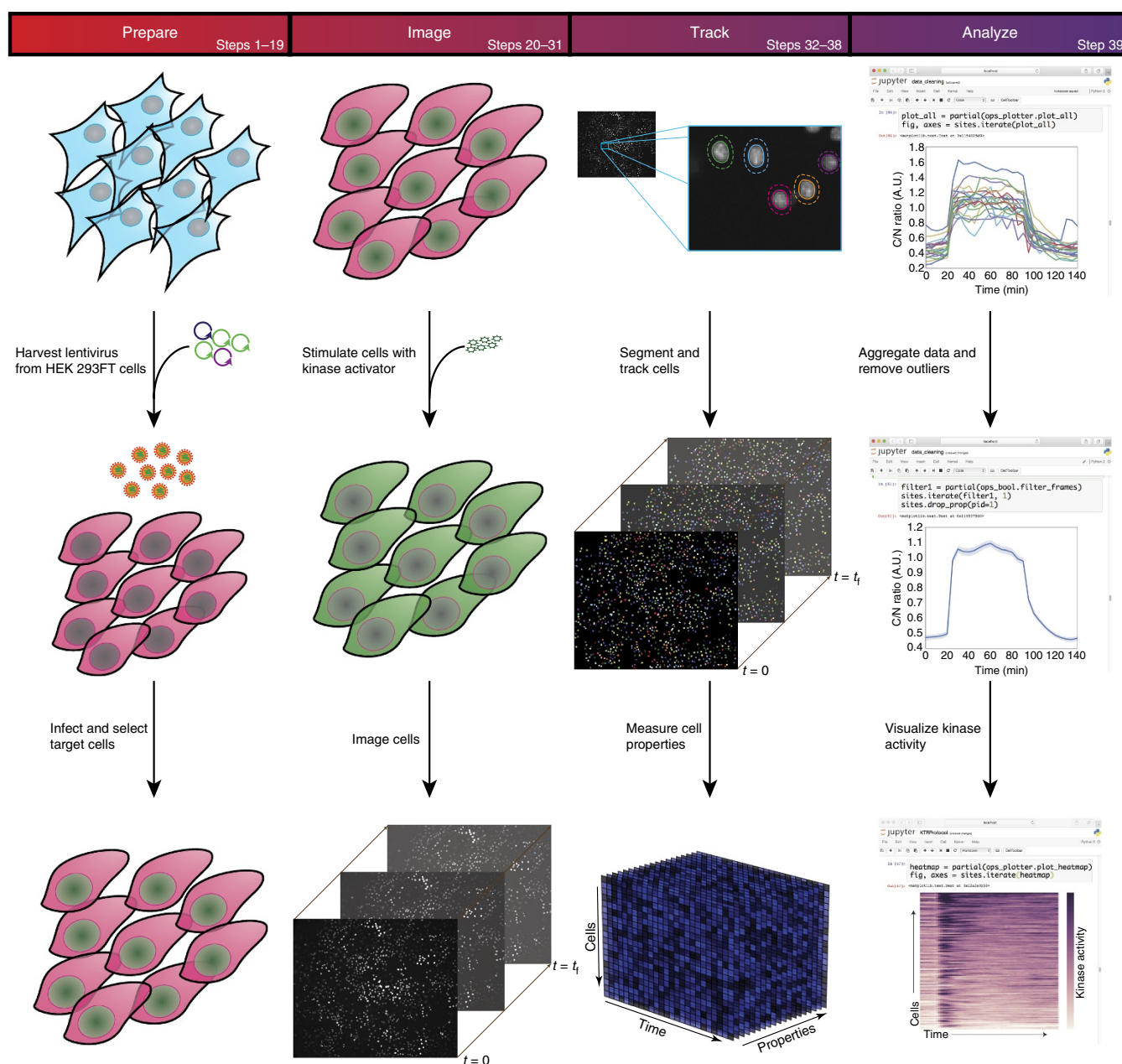


Figure 2 | General schematic showing how live-cell measurements of kinase activity are performed using kinase translocation reporters (KTRs). First, lentivirus containing the KTR is made in 293FT cells and used to infect the cell type of interest. Infected cells are selected, treated with a kinase activator, and imaged with a fluorescence microscope. Cells are identified, segmented, and tracked from the resulting images. Finally, cell properties such as fluorescence intensity and localization are measured and used to estimate kinase activity.

Box 1 | Design of the NES and bNLS sequences

The KTRs require the NES and bNLS sequences to be located near the phosphorylation motif. Typically, the activity of the bNLS is suppressed, whereas the activity of the NES is enhanced by phosphorylation of sites nearby. Both bNLS activity suppression and NES activity enhancement shift the equilibrium location of the KTR constructs from the nucleus to the cytoplasm. To achieve an optimal dynamic range, the import rate and export rate must be well-balanced and yet large enough for sufficient translocation to occur. Here, we explain some rules that determine the strength of import and export for KTRs.

Nuclear export signals

The consensus NES sequences used in KTRs are $\Phi\text{XXX}\Phi\text{XX}\Phi\text{X}\Phi$, where Φ denotes any hydrophobic amino acid and X denotes any amino acid (Fig. 3)¹⁷.

To tune the export rate, we suggest the following general rules:

1. Amino acids at positions +0, +4, +7, and +9 can be substituted for hydrophobic residues (L, I, V, and M).
2. Hydrophobic residues at position +0 can also be substituted with F, W, C, T, and A, leading to slightly reduced export rate.
3. Incorporating negatively charged amino acids at positions −3 to −1 and +1 to +3 enhances the export rate. Phosphorylation residues should be placed in these regions.
4. Proline at positions +3, +5, +6, and/or +8 lowers the export rate.
5. Having more than two hydrophobic residues in positions +1 to +3 or positions +4 to +5 lowers the export rate.

Nuclear localization signals

Among several classes of NLS, a bipartite NLS was shown to control its import rate upon phosphorylation or charged amino acid substitution in the most consistent manner¹⁰. For simplicity, we define the first basic amino acid as position +0 and assume the regions between bipartite basic amino acids are 10 aa in length, although they can vary between 10 and 12 aa (Fig. 3).

To control the import rate, we suggest the following general rules:

1. The first basic amino acids (position +0 and +1) should be KR. RRR or RRK can also be used as needed. The optimal terminal amino acids are KK, KR, K, or R. The choices of these initial and terminal basic amino acid residues are critical for bNLS activity.
2. Phosphorylation at +2, +3, +4, +9, +10, and +11 or −1, −2, and −3 can disrupt nuclear import¹⁸.
3. Acidic amino acids included within +5 to +10 increase the import rate, and hydrophobic and basic amino acids in this region decrease the import rate.

Note that amino acid substitution or sequence engineering often fails to mimic the phosphorylation effects in other types of NLSs present in naturally occurring proteins¹². For example, a phosphomimetic mutation does not always reproduce localization changes that would be produced by phosphorylation.

the analysis, and the models needed to extract parameters are somewhat unique to each kinase. They are also dependent on the availability of parameter values from the literature and experimental tools (e.g., the availability of specific kinase inhibitors). We demonstrate a quick workflow specific to our JNK KTR, which is illustrative of the overall process that would be performed for other KTRs (Supplementary Notes 1 and 2).

Experimental design

We explain how to prepare the reporter cell line and how to perform live-cell imaging (Fig. 2). The KTR development process is specific to each kinase. There are some important considerations to keep in mind when developing a new KTR; these are described in the sections below. We also describe how to model absolute kinase concentrations in single cells by analyzing live-cell imaging data.

Selecting substrates. A kinase of interest needs to phosphorylate its KTR, so we begin by selecting a few substrates with phosphorylation sites that are phosphorylated by the kinase with high specificity (e.g., c-Jun is a good substrate for JNK). Databases of known substrates are useful in this regard²⁶.

Selecting a cell culture system. Choose a cell line that has a functional signaling pathway for the kinase of interest (as expression of many receptors is cell dependent) and that will be receptive

to the KTR constructs via transfection or lentiviral infection. Adherent cells that have a large cytoplasmic region are also preferred because translocation can be more readily assessed microscopically. We typically use NIH/3T3 fibroblasts, HEK293 cells, or HeLa cells for KTR development. We also recommend using a previously validated KTR in each new cell line as a control for dynamic range and functionality. Phosphomimetic and nonphosphorylatable mutants can be used for measuring dynamic range regardless of the basal kinase activity in the cell line. We have made some tools for this purpose, available through Addgene (Supplementary Table 1).

Determining a perturbation strategy. A kinase of interest must be activated or inactivated to cause KTR translocation. A stimulant should be chosen based on the biological contexts to be investigated, as it may narrow down a scope of specificity to be optimized. Specific perturbations should also be identified to enable evaluation of specificity. Inhibitor treatment using small molecules is easy and convenient, but often not available. Gene knockdown or knockout using RNAi- or CRISPR-based techniques could also serve as perturbations, but they are more time-consuming and typically require more validation of efficacy.

Incorporating bNLS and NES sequences. KTRs must be phosphorylated by a kinase of interest—yet they also must have

bNLS and NES sequences around the phosphorylation site that are strong enough to induce translocation without inhibiting phosphorylation events (see **Box 1** and Experimental design for details of how this is achieved). Mass spectrometry or a mobility shift assay can be used to ensure that a KTR is still phosphorylated upon kinase activation^{27,28}.

The mechanism of substrate recognition is kinase-dependent. For example, MAPKs and CDKs are proline-directed kinases that require a phosphorylation residue to be followed by a proline, and these kinases also recognize their substrates by distal docking sites. Such features are suitable for designing specific and sensitive KTRs, because the mutations around the phosphorylation site are less likely to affect kinase substrate recognition. In addition, it is straightforward to incorporate multiple phosphorylation sites into the KTRs for these kinases due to the relatively simple target residue requirement (i.e., serine followed by proline). Accordingly, several of these KTRs are available, including those for ERK, JNK, p38, and CDK2 (**Table 2**).

By contrast, for many other kinases, multiple amino acids around the phosphorylation site, typically four amino acids on either side, contribute substantially to kinase substrate recognition²³. As a result, there may sometimes be a trade-off between the efficiency of substrate recognition and nuclear–cytoplasmic shuttling when the sequence used for substrate recognition is located proximally to the bNLS and NES sites. Furthermore, in some cases the native target sequence contains fewer phosphorylation sites than required (e.g., only one site is found, but sites for both a bNLS and an NES are desired). If the design requires additional phosphorylation sites, an additional element may be

added to improve the dynamic range, such as incorporating a repeated consensus phosphorylation motif, as was implemented in the PKA KTR¹⁰.

Identifying the minimal substrate sequence. Truncation of natural kinase substrates can reduce off-target biological effects when the KTR is expressed—but possibly at the cost of specificity. As mentioned above, the mechanism of substrate recognition must be taken into account; for example, a distal docking site is required for JNK KTR to be recognized by JNK.

If available, an antibody against the phosphorylation site can be used to determine minimal sequences, which still receive phosphorylation by the kinase. Moreover, if functional domains (e.g., the DNA-binding domain) have been identified in the substrate sequences, they should be removed if possible.

Assessing translocation and redesign if necessary. After designing the sequences, it typically takes a week for a lentiviral plasmid cloning and another 1–2 weeks to assess translocation in cells. If translocation is observed upon addition of stimulants or inhibitors, it is likely that the KTRs report the activity of the kinase of interest. In many cases, translocation is visually obvious. If a KTR shows little or no translocation, there are three possible causes: (i) the reporter is not phosphorylated because the perturbation strategy is not sufficient to produce changes in kinase activity; (ii) the reporter is not phosphorylated because the bNLS and/or NES inhibit phosphorylation; or (iii) the reporter is phosphorylated, but the localization signals are not strong enough to cause translocation. Some optimization insights and strategies are given in

TABLE 2 | Frequently used nuclear/cytoplasmic translocation-based mammalian signaling reporters.

Reporter name	Pathway	Comments
ERK KTR ^{10,14,35}	ERK	
JNK KTR ¹⁰	JNK	
p38 KTR ¹⁰	p38	
PKA KTR ¹⁰	JNK	
p65-FP ^{4,36}	NFκB	Nuclear localization indicates increased activity
MK2-FP ^{37–39}	p38	MK2 missing the first 31 aa was used ³⁷
STAT1-FP, STAT3-FP ⁴⁰	STAT	Endogenous fusion of STAT1-GFP and RFP-STAT3 was done through genome editing. Nuclear localization indicates increased activity
NFAT1-FP, NFAT4-FP ⁴¹	NFAT	These are more active when they are in the nucleus
FoxO1-FP, FoxO3-FP ^{14,42–44}	Akt	DNA-binding activity and Mst1 phosphorylation were disrupted by point mutations in FoxO1 (refs. 42,44) The C-terminal region of FoxO3 was removed, and a point mutation was further introduced to disrupt the DNA-binding domain ¹⁴
SMAD2-FP ^{45,46}	TGF-β/SMAD	Nuclear localization indicates increased activity
DHB ^{8,47}	Cdk2	Only the C-terminal 94 aa of DNA helicase B were used ⁴⁷
YAP1 (refs. 8,48)	Hippo	Nuclear localization indicates increased activity
ERK-FP ⁴⁹	ERK	ERK was endogenously tagged by introducing YFP as an exon in the ERK2 gene. Nuclear localization indicates increased activity

PROTOCOL

Box 1; remember that phosphomimetic and nonphosphorylatable mutants may be useful for optimizing dynamic range by enabling one to test the effect of several phosphorylation residues in an independent manner.

Image processing. To quantitatively evaluate kinase activity, the C/N ratios must be calculated from time-lapse images. Using the C/N ratio allows us to normalize the variability of expression level between cells. To obtain these measurements, the nucleus and cytoplasm for each individual cell must be located and segmented. Nuclei are relatively easy to segment because their boundaries are clearly defined. The cytoplasmic boundary is not as well defined, especially with confluent cells, in which case cells are frequently in contact or overlapping. As a result, we use the nuclear boundaries as the basis for segmenting the cytoplasm as well. After locating the nucleus, the boundary of the nucleus is expanded by a few pixels in each direction. The ring that is formed by this dilation is used as a proxy for the cytoplasm. This region can be further corrected by removing background pixels, if needed. Although we use this method most frequently, it is worth noting that a new open-source, deep-learning method for whole-cytoplasmic segmentation has been developed and applied to KTR quantification²⁹.

The typical workflow for quantification is the following: first, nuclei are segmented based on Hoechst staining or H2B-fused fluorescent proteins. Next, the cytoplasm is segmented by dilating a few pixels away from the defined nucleus. The C/N ratio is calculated by dividing the median cytoplasmic KTR intensity by median nuclear KTR intensity.

These analyses, including cell tracking, can be implemented using readily available image analysis software such as Fiji and

CellProfiler^{30,31}. In this protocol, we introduce our pipeline for a flexible live-cell image analysis using our open-source software, CellTK. Adjustable parameters and algorithms allow for optimization of segmentation and tracking to the cell type and plating density used (Steps 32–39).

Data visualization and modeling of absolute kinase concentrations. In most cases, obtaining single-cell resolution C/N ratios requires removal of outlier cells that express very low levels of the reporter, are unusually large or small, or divide or die during imaging. The process we use to accomplish this is presented in the **Supplementary Methods and Supplementary Note 1**.

As a further application, we also describe how to use the obtained C/N ratio to estimate single-cell level absolute concentration of active kinase over time. Briefly, the C/N ratio is determined for cells expressing either a phosphomimetic (e.g., constitutively active) or nonphosphorylatable (constitutively inactive) version of the KTR, or the wild-type construct. These cells are then subjected to multiple perturbations to determine parameter values for an ordinary differential equation-based mathematical model of KTR translocation. For example, treating these cells with leptomycin B inhibits nuclear export and thus enables determination of the nuclear import rate for both phosphorylated and nonphosphorylated KTRs. With knowledge of these nuclear import rates and translocation data obtained before leptomycin B treatment, it is also possible to calculate nuclear export rates. Full details of this process using our JNK KTR are given in the **Supplementary Methods and Supplementary Note 2**; note that the modeling approach is highly specific to the kinase of interest, and also that feasibility of this approach is highly dependent on available molecular tools.

MATERIALS

REAGENTS

- Cells of interest. We used the 293FT cell line (Fisher Scientific, cat. no. R70007) for virus production. We used NIH/3T3 cells (ATCC, cat. no. CRL-1658) as target cells, but our approach can also be used with RAW 264.7 cells (ATCC, cat. no. TIB-71), HeLa S3 cells (ATCC, cat. no. CCL-2.2), or any other adherent cells of interest with a large cytoplasmic region (see 'Experimental design') **! CAUTION** The cell lines used in your research should be regularly checked to ensure they are authentic and are not infected with mycoplasma.

Cell culture

- DMEM, high glucose, L-glutamine (Life Technologies, cat. no. 11965092)
- FBS (Clontech, cat. no. 631106)
- L-Glutamine (Life Technologies, cat. no. 25030081)
- Penicillin–streptomycin solution (Life Technologies, cat. no. 15140-163)
- PBS, pH 7.4 (Life Technologies, cat. no. 10010023)
- Trypsin–EDTA (0.05% (wt/vol)) (Life Technologies, cat. no. 25300120)
- 5% sodium hypochlorite solution (household bleach; Clorox)

Lentiviral production and infection

- A panel of lentiviral vectors encoding KTRs and the H2B fused to different fluorescent proteins are available through Addgene (**Supplementary Table 1**). The promoter strength should be chosen based on the specific imaging application, but as long as the signal-to-noise ratio is sufficient, a weaker promoter is preferable to minimize potential nonspecific perturbations in the cell. We typically recommend a PGK promoter, which provides a suboptimal expression level and enough dynamic range in many cell lines (**Supplementary Fig. 1**). A lentiviral plasmid sequence encoding a JNK KTR under PGK promoter control can be found in the **Supplementary Data**
- VSV-g vector (Addgene, cat. no. 8454)
- Δ8.2r vector (Addgene, cat. no. 8455)

- Opti-MEM reduced-serum medium (Life Technologies, cat. no. 31985088)
- Lipofectamine 2000 (Life Technologies, cat. no. 11668019)
- Polybrene (EMD Millipore, cat. no. TR-1003-G)
- Puromycin solution (InvivoGen, cat. no. ant-pr-1)
- Blasticidin solution (InvivoGen, cat. no. ant-bl-1)

Imaging

- Fibronectin from human plasma, 0.1% (wt/vol) solution (Sigma-Aldrich, cat. no. 86088-83-7)
- FluoroBrite DMEM, high glucose, 3.7 g/liter sodium bicarbonate (Life Technologies, cat. no. A18967-01)
- Hoechst 33342 dye, 10 mg/ml (Fisher Scientific, cat. no. H3570)
- 5% CO₂ gas blend (e.g., Praxair, cat. no. BI NICD5O6-K)

Data analysis software

- Docker (<https://www.docker.com/>). If your machine is running Windows 7 (or previous), we recommend using VirtualBox (<https://www.virtualbox.org/>) to first install Ubuntu v16.04.1 or later
- Python (v2.7.13, <https://www.python.org/downloads/>). This software is pre-installed in the Docker environment
- CellTK (v0.3, <https://github.com/braysia/CellTK>). This software is pre-installed in the Docker environment
- Covertrace (v0.1, <https://github.com/CovertLab/covertrace>). This software is pre-installed in the Docker environment
- Fiji (<http://fiji.sc/>).

EQUIPMENT

- 0.22 μm sterile vacuum filtration system (Millipore EMD, cat. no. SCGPU05RE)
- Sterile flow hood (e.g., Labconco, Purifier Logic+ Class II model)
- Humidified 37 °C, 5% CO₂ incubator (e.g., Heracell 150i; Thermo-Fisher Scientific)

- 1.5-ml Microcentrifuge tube (Corning, cat. no. MCT-150-C-S)
- 6 ml-Luer-lock-tip syringe (Covidien, cat. no. 8881516937)
- 0.45- μ m SFCA Nalgene syringe filter (Life Technologies, cat. no. 723-2545)
- 15-ml Polypropylene conical tube (Corning, cat. no. 352096)
- Six-well polystyrene tissue culture plates (Corning, cat. no. 353046)
- 96-Well optical-bottom plates with coverglass base (Life Technologies, cat. no. 164588)
- 8-Well coverglass slide (Life Technologies, cat. no. 155411)
- Microscope: Any inverted microscope setup that allows for environmental control, fluorescence imaging, and automatic positioning can be used. We used a Nikon Eclipse Ti-E inverted microscope with an Andor Neo 5.5 sCMOS Camera for all of our imaging. If possible, we recommend the use of a microscope with an autofocus system, as this will allow for consistently higher-quality images. We also used a Sutter Instrument light source (cat. no. LB-LS/30) and an Applied Scientific Instrumentation motorized stage (cat. no. MS-2000) to allow for automated image acquisition at multiple time points and in multiple channels
- Microscope incubator: We used a Haison microscope incubator designed for the Nikon Ti-E to establish a controlled environment. We used a World Precision Instruments Air-Therm ATX heater controller for temperature control and commercially available 5% CO₂ gas cylinders (e.g., Praxair, cat. no. BI NICD506-K) for atmospheric control. To reduce evaporation for long imaging experiments, the gas is humidified by bubbling through water before being introduced to the chamber

REAGENT SETUP

DFPG growth medium Add (in order) 500 ml of high glucose, L-glutamine DMEM, 50 ml of FBS (10% (vol/vol)), 5 ml of 66 mM L-glutamine, and 5 ml of the penicillin–streptomycin solution to a 0.22- μ m sterile vacuum filter and filter sterilize. Store the solution at 4 °C and use within 1 month.

FBS imaging medium Prepare all reagents in sterile conditions. Add 1% (vol/vol) FBS and 1% (vol/vol) L-glutamine to a volume of FluoroBrite DMEM. Store the solution at 4 °C. Make new FBS imaging medium for each imaging experiment.

EQUIPMENT SETUP

Imaging filters The correct imaging filters to use will depend on the fluorescent proteins and nuclear stains used. **Table 1** details the filters that are regularly used in our lab. For this combination of filters and fluorescent proteins, bleed-through should be negligible, and thus spectral unmixing is not needed.

Image acquisition We use the open-source software Micro Manager for image acquisition³². We have used both version 1.4.x and version 2.0.x (beta) successfully. The software allows for automatic setup of imaging using multiple filters in multiple positions. First, the user manually selects and

saves the coordinates on the plate to be imaged. Next, the user defines the magnification and binning, the interval between images, the filters, and the exposure times to be used.

The proper magnification to use will depend on the image resolution desired and the cell type used. Larger magnifications allow for more detail, but the smaller field of view means that data will be collected from fewer cells. Similarly, greater binning reduces detail but increases the signal. In general, we use either a 10 \times objective with 1 \times 1 or 2 \times 2 binning, or a 20 \times objective with 2 \times 2 or 3 \times 3 binning.

We recommend taking some still images to adjust the exposure times. In each still image, locate some of the brightest cells and ensure that the pixels are not saturated by viewing the histogram. Images should be collected in a lossless format. We use 16-bit TIF images.

We typically select two to three locations per well for imaging. Locations should be selected such that as many cells as possible are present, without many cells overlapping or in contact. Overly confluent cells can lead to mis-segmentation or overlapping cells that must be cleaned later, or even to a change in cellular behavior. The selection of more locations per well increases the amount of data collected per well but also decreases the number of wells that can be imaged over a fixed time interval.

The interval between images should ideally be as short as possible for greater temporal resolution. However, time is required to allow the automated stage to move to each subsequent imaging position. In addition, certain wavelengths of light can be phototoxic. In the case of cell death due to phototoxicity, it may be necessary to lengthen the interval between images and/or reduce the intensity of the excitation light. Other solutions, such as optimizing the excitation spectra with more precise filters or improving hardware synchronization, can also be helpful³³.

Before initiating the experiment, we recommend allowing the microscope to image all the locations once. This will allow the user to confirm that the microscope is functioning properly and that the stage has time to image all the locations before the next time point.

Setup a Docker container We provide the Docker image for users to reproduce the computational analysis. First, download Docker, which is available from <https://www.docker.com/>. If your machine is running Windows 7 (or previous), we recommend using VirtualBox (<https://www.virtualbox.org/>) to install Ubuntu v16.04.1 or later. Install and run the Docker image for this protocol. This will install all of the required software and packages. An empty working directory should be specified by users, referred to here as \$WORKDIR. To do this, open a terminal and type the following command: `docker pull braysia/ktrprotocol`

PROCEDURE

Production of lentivirus in HEK 293FT cells ● TIMING 3 d

1 | One day before transfection, plate $\sim 4 \times 10^5$ 293FT cells in each well of a six-well tissue culture plate in 1.5 ml of DFPG growth medium.

▲ **CRITICAL STEP** Cells should be <70% confluent and of low passage number at the time of transfection to maximize lentiviral production.

2 | Prepare the transfection solution in a 1.5-ml microcentrifuge tube: add (in order) 25 μ l of Opti-MEM, 0.75 μ g of Δ 8.2r, 0.25 μ g of VSV-g, and 1.0 μ g of the lentivector containing the KTR of interest. Flick the tube gently to mix the solution after each addition.

▲ **CRITICAL STEP** To check the dynamic range of the KTR, prepare transfection solutions to transfect AA and EE mutants of the KTR of interest. For the KTR presented in the ANTICIPATED RESULTS section, we used JNK KTR AA (Addgene, cat. no. 90238) and JNK KTR EE (Addgene, cat. no. 90239) as the controls.

3 | In a separate 1.5-ml microcentrifuge tube, add 150 μ l of Opti-MEM.

4 | Add 6 μ l of Lipofectamine directly to the Opti-MEM and flick the tube gently to mix the solution. Incubate the solution at room temperature (20–23 °C) for 5 min.

▲ **CRITICAL STEP** Avoid direct contact of Lipofectamine 2000 with the sides of the microcentrifuge tube, as this will lead to lower transfection efficiency.

PROTOCOL

- 5| Add the solution from Step 4 to the solution from Step 2 and flick the tube gently to mix.
- 6| Incubate the solution at room temperature for 20 min.
- 7| Apply the transfection solution directly to the cells dropwise and rock the plate gently to mix.
- 8| Incubate the cells at 37 °C and 5% CO₂ for 48 h.

! CAUTION The supernatant of the transfected HEK 293FT cells will contain infectious lentiviral particles. Lentiviruses can infect human cells, and enhanced Bio-safety level II containment is recommended by the National Institutes of Health (NIH). Lab coats and double gloves should be used, and anything exposed to the lentiviral solution should be soaked in 10% (vol/vol) bleach for 30 min before discarding.

- 9| One day after transfecting the HEK 293FT cells, plate the target cells in a six-well plate so that they will be between 30% and 50% confluent on the day of infection.

Harvest of lentivirus ● **TIMING** ~1 h—1 d, depending on whether additional virus is harvested

- 10| Using a microscope, observe the cells from Step 8. The cells should be fluorescent, and transfection efficiency should be >70%. It is normal for cells to detach easily from the surface of the plate at this stage.

? **TROUBLESHOOTING**

- 11| Using a 6-ml syringe in a biological safety cabinet, aspirate the supernatant from each well.
- 12| Filter the solution through a 0.45-µm SFCA syringe filter into a 15-ml conical tube. The lentiviral solution can be concentrated by centrifugation at 120,000g for 60 min at 4 °C, discarding the supernatant.
- 13| (Optional) More lentivirus can be collected by adding another 1.5 ml of DFGP growth medium to the cells immediately after harvesting the lentivirus. Incubate the cells at 37 °C and 5% CO₂ for 24 h and repeat Steps 11 and 12. The virus can be stored or pooled with the solution from Step 12.
▲ **CRITICAL STEP** The cells are very sensitive at this stage. The time between harvesting lentivirus and replacing medium should be kept as short as possible. The medium should be added slowly to prevent cells from detaching.
■ **PAUSE POINT** The solution can be stored at –80 °C for 6 months or at 4 °C for 5 d. As either storage method will reduce infection efficiency, we recommend using the lentiviral solution immediately to infect cells (Step 14).

Infection of target cells

- 14| Infect the target cells from Step 9 either without (option A) or with (option B) spinning in a centrifuge. Spin treatment can increase infection rates, especially with cell lines that are difficult to infect, such as RAW 264.7. Spin treatment requires a centrifuge with a rotor capable of spinning tissue culture plates.

(A) Infection without spin treatment ● **TIMING** 20 min

- (i) Add DFGP growth medium to the lentiviral solution (from Step 12 or 13) to bring the volume up to 2 ml (or 4 ml, if using solution from Step 13).
- (ii) Add Polybrene (10 mg/ml) to the solution such that the final concentration is 10 µg of Polybrene per ml of lentiviral solution (either 2 or 4 µl).
- (iii) Aspirate the medium from the target cells and replace it with the lentiviral solution.
- (iv) Incubate the cells at 37 °C and 5% CO₂. Wait at least 24 h post infection before beginning selection in Step 15, to allow the antibiotic resistance genes to be expressed.

(B) Infection with spin treatment ● **TIMING** 90 min

- (i) Preheat a centrifuge capable of spinning tissue culture plates to 32 °C.
- (ii) Add DFGP growth medium to the lentiviral solution (from Step 12 or 13) to bring the volume up to 4 ml.
- (iii) Add Polybrene (10 mg/ml) to the solution such that the final concentration is 10 µg of Polybrene per ml of lentiviral solution (4 µl).
- (iv) Aspirate the medium from the target cells and replace it with the lentiviral solution.
- (v) Transfer the plate with the target cells and lentivirus to a preheated centrifuge. Centrifuge the cells at 1,600g and 32 °C for 60–100 min.
- (vi) Incubate the cells at 37 °C and 5% CO₂. Wait at least 24 h post infection before beginning selection in Step 15, to allow the antibiotic resistance genes to be expressed.

Selection of infected cells ● **TIMING** 2–5 d

15| After 24 h, aspirate the lentiviral solution from the cells and immediately replace it with 2 ml of DFIG growth medium with the appropriate antibiotic for selection. The concentration of antibiotic to use is dependent on the cell type and the expression of the resistance gene. We typically use 1–5 µg/ml puromycin, 1–5 µg/ml blasticidin, or 25–100 µg/ml hygromycin. For data presented in the ANTICIPATED RESULTS section, we selected cells using puromycin. In addition, apply antibiotic to uninfected target cells to use as a reference for the efficacy of selection.

▲ **CRITICAL STEP** If a cell line is not suitable for antibiotic selection, fluorescence-positive cells can be sorted with flow cytometry³⁴.

? **TROUBLESHOOTING**

16| (Optional) Trypsinize and transfer some of the cells (~200 µl) to an 8-well coverglass slide and cover with PBS or FBS imaging medium. Image with a fluorescence microscope to visually estimate the infection rate. This will make it easier to evaluate the success of the selection, as the proportion of surviving cells should be approximately equal to the proportion of infected cells. We usually obtain infection rates of 50–70% in HeLa S3, NIH/3T3, and RAW 264.7 cells.

▲ **CRITICAL STEP** Cells without reporter expression can also be computationally removed during data analysis. In this case, the amount of data obtained will be dependent on the infection rate.

17| Regularly inspect the cells under a microscope for dead cells to confirm successful selection. Cell death should be observed 48 h after beginning selection with puromycin and 72–96 h after beginning selection using hygromycin or blasticidin.

? **TROUBLESHOOTING**

18| Transfer the selected cells to a new well without antibiotics to allow the KTR-expressing cells to recover.

19| Incubate the cells at 37 °C and 5% CO₂ for 24–48 h.

Plating of cells for imaging ● **TIMING** 1–5 h

20| To improve cell adherence and viability, the optical-bottom plates must be treated with fibronectin. Dilute the fibronectin solution 1:100 (vol/vol) in PBS.

21| Add 55 µl of the fibronectin solution to each well of an optical-bottom 96-well plate that is going to be imaged, and ensure it covers the entire well.

22| Incubate the plate at 37 °C for 1–4 h.

23| Aspirate the solution from the wells and add 200 µl of PBS.

24| Repeat Step 23 two more times.

■ **PAUSE POINT** The fibronectin-coated wells can be kept at 4 °C in PBS buffer for 1 week.

25| Aspirate the PBS and plate 7,000–20,000 (number is cell-type-dependent) cells in 100–200 µl of DFIG growth medium in each fibronectin-coated well, such that they will be 30–50% confluent 12–24 h later for imaging. NIH/3T3 cells were plated at 7,000 cells per well to collect the data shown in **Figure 3**. Leave the cells to adhere at room temperature for 10–15 min before moving them to a 37 °C, 5% CO₂ incubator.

Live-cell imaging ● **TIMING** 2–8 h

26| Six hours before imaging, replace the medium on the cells with 100 µl of FBS imaging medium so that the kinase activity has time to reach steady state in the new environment.

▲ **CRITICAL STEP** The 6 h duration of starvation can be condition-dependent; the duration or necessity of serum starvation should be determined for each individual assay. We recommend using 1% (vol/vol) FBS imaging medium to reduce background signal, but this is not strictly necessary.

27| For imaging experiments shorter than a couple of hours, use a Hoechst nuclear dye for nuclear segmentation. Prepare a 50 µg/ml dilution of Hoechst in H₂O. One hour before imaging, add this solution 1:1,000 (vol/vol) to the wells containing the cells to be imaged and incubate for 1 h at 37 °C and 5% CO₂. Aspirate the medium containing the stain, wash the cells once with 200 µl PBS, and add 100 µl fresh imaging medium. Note that Hoechst staining can cause genotoxic stress, so it might not be appropriate for certain assays.

PROTOCOL

▲ CRITICAL STEP For imaging experiments longer than a couple of hours, we recommend using an H2B-fused fluorescent protein for nuclear segmentation (**Supplementary Table 1**).

28| Image the cells on an inverted fluorescence microscope in a 37 °C, 5% CO₂ environment. A 20× objective with 3 × 3 binning in a 16-bit format provides many cells (~750–1,000 RAW 264.7 cells or 200–300 HeLa cells) in the field of view and enough detail to see cytoplasmic and nuclear translocation for most cell types. Use the appropriate excitation and emission filters for the fluorescent protein in the KTR (**Table 1**). For example, for YFP proteins (such as the JNK KTR-mClover, see **ANTICIPATED RESULTS**) we use an excitation filter with 500 ± 20 nm transmission and an emission filter with 535 ± 30 nm transmission.

? TROUBLESHOOTING

29| Determine the optimal duration of imaging, which is dependent on the experimental assay, and ensure this to be long enough to capture the entire dynamic range of kinase activation or deactivation. The interval between images is also dependent on the specifics of the assay. Use of shorter intervals will provide better temporal resolution and make tracking cells easier, but it increases the risk of phototoxicity. We typically image cells for 2–6 h with intervals no longer than 15 min.

▲ CRITICAL STEP Exposure conditions should be chosen so that the dynamic range is as large as possible. The light intensity used to generate a sufficient signal-to-noise ratio may lead to phototoxicity and photobleaching. The simplest way to reduce phototoxicity while preserving signal-to-noise ratio is to increase the time interval between images or use a less intense light with a longer exposure time. Longer wavelengths are less phototoxic, and thus we have never experienced phototoxicity issues with KTRs fused to mClover or mRuby2 in our applications (**Supplementary Table 1**). Phototoxicity can also be reduced by using filters with more precise ranges or by improving the synchronization between microscope components. There are a number of ways to measure phototoxicity³³; these can be useful in assessing the effectiveness of any reduction strategy. Our typical approach is to monitor the overall movement of cells; unhealthy cells tend to move much less.

30| Capture several images before stimulating or inhibiting kinase activity to establish the initial steady-state KTR profile. Replace all or part of the medium in the dish with medium containing the stimulant. For the data presented in the **ANTICIPATED RESULTS** section, we replaced the medium with 100 µl of FBS imaging medium containing stimulants. Align the plate to the previous position when returning it to the microscope. Acquire images at regular time intervals to assess the effect of the stimulant or inhibitor on kinase activity. Save the files in TIF format.

31| Take several images from a well without cells, but containing the same imaging medium. These images should be used as a background reference to detect camera offset, medium autofluorescence, and illumination bias. However, for long imaging experiments (>5 h), the presence and abundance of cells can affect the degree of medium autofluorescence, and, therefore, the background signal. The background can be computationally estimated as well (**Supplementary Methods**).

Data analysis ● TIMING 1–5 d

32| Visually assess the images for translocation subsequent to kinase activator/inhibitor treatment.

33| Use CellTK to segment images and extract single-cell properties. The steps below describe an example with a test data set we provide. Install Docker (<https://www.docker.com/>), which will be used to install all of the necessary software packages (Equipment Setup).

34| Set a location that will be used as the working directory (subsequently referred to as \$WORKDIR). Use Docker to install the necessary packages in \$WORKDIR by typing the following command in a Terminal window:

```
docker run -it -v $WORKDIR:/home/ braysia/ktrprotocol
```

35| Download and extract the example image data sets using the Terminal command below:

```
wget http://archive.simtk.org/ktrprotocol/KTRimages.zip && unzip KTRimages.zip
```

The extracted folder contains images of NIH/3T3 cells from the published experiments presented in the **ANTICIPATED RESULTS** section. The files are explained in **Supplementary Table 2**.

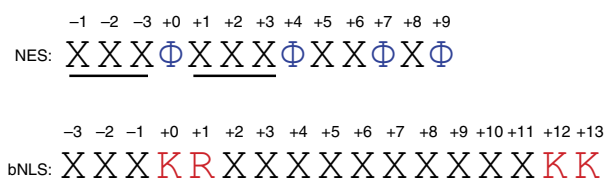


Figure 3 | NES and bNLS consensus sequences. Hydrophobic (blue) and basic (red) amino acids are indicated, where Φ denotes any hydrophobic amino acid and X denotes any amino acid; underlining indicates potential phosphorylation residues.

36| Download and extract the configuration files for image processing. The configuration files are located in input_files/ktr_inputs:

```
wget http://archive.simtk.org/ktrprotocol/input_files.zip && unzip input_files.zip
```

Experimental data sets will require new configuration files to be written in the YAML format (<http://www.yaml.org/start.html>). A detailed description of the configuration file structure is provided in the CellTK documentation (README.md and doc/CONFIGURE_YML.md). In short, the configuration file specifies which operations will be run on the images, the parameters necessary for those operations, and where the outputs are saved. The operations used to analyze the example data sets are described in **Supplementary Table 3**.

37| Run CellTK using each of the provided input files. The output files, which include segmented images and extracted single-cell properties, will be stored in /home/output in the Docker environment, or \$WORKDIR/output in the mounted working directory.

```
celltk -n 3 input_files/ktr_inputs/input_*.yaml
```

▲ CRITICAL STEP The expected runtime is ~1 h using three cores of a 2.2-GHz Intel Core i7 MacBook Air. The integer after ‘-n’ can be substituted with any number of cores for parallelization. We recommend optimizing the parameters in the configuration file on a small subset of images before running CellTK on the entire data set.

38| Inspect the output nuclear and cytoplasmic tracking images (e.g., /home/output/AnisoInh/Pos0/nuc and /home/output/AnisoInh/Pos0/cyto) to ensure accurate tracking. Adjust parameters in the input files as needed.

▲ CRITICAL STEP Generating good data requires accurate segmentation and tracking of the images. Tracking images should be largely devoid of segmentation errors (non-labeled cells and artifacts labeled as cells). Fiji (<https://imagej.net/Fiji/Downloads>) can be used to view the images (*File > Import > Image Sequence*). Use the ‘glasbey inverted’ lookup table (*Image > Lookup Tables > glasbey inverted*) to visualize tracking. Each individual cell should remain a single color for each image in the time series.

39| Use the extracted cell properties to obtain a quantitative C/N ratio for the entire time series for each cell (see Equipment Setup and **Supplementary Methods** sections for further details).

? TROUBLESHOOTING

Troubleshooting advice can be found in **Table 3**.

TABLE 3 | Troubleshooting table.

Step	Problem	Possible reason	Solution
10	Low transfection efficiency	Endotoxin or other toxins in purified DNA	Purify DNA using endotoxin-free kits. Avoid protocols that include phenol/chloroform extraction
		DNA/transfection reagent ratio is sub-optimal	Vary DNA/Lipofectamine 2000 ratio from 1:0.5 to 1:5
		High passage number of HEK 293FT cells	Use cells with passage number < 10
		Suboptimal confluency of HEK 293FT cells	Use cells that are 30–60% confluent at the time of transfection
15	Low infection efficiency	The cell type of interest is difficult to infect	Some cell types are difficult to infect without spin treatment. Poor infection rates can sometimes be improved by performing the infection with spin treatment

(continued)

TABLE 3 | Troubleshooting table (continued).

Step	Problem	Possible reason	Solution
17		Poor virus quality	Ensure 293FT cells are healthy and of low passage number for viral production. Cells that are allowed to grow to confluency produce lower viral titers Additionally, the lentiviral solution can be concentrated by ultracentrifugation (Step 12)
		Cellular anti-viral response	Some cell types, such as Raw 264.7 cells, have innate immune systems to resist viral infection. Some reagents, such as ViralPlus (ABM, cat. no. G698), can help counteract this and improve infection rates
	Poor selection—many false positives	Low antibiotic concentration	Increase the amount of antibiotic used in selection. Ensure that the antibiotic has not degraded in storage (for example, by repeated freeze–thaw cycles)
	Poor selection—few cells survive	High antibiotic concentration	Decrease the amount of antibiotic used in selection
	Poor selection—cell death sooner than expected	High antibiotic concentration	Minimal cell death should be observed until the times specified. Use a lower concentration of antibiotic if cell death is observed sooner
28	Cell death during imaging	Phototoxicity	The intense light used to generate a sufficient signal-to-noise ratio may lead to phototoxicity. Phototoxicity can be reduced while preserving signal-to-noise ratio by using less intensity and a longer exposure time or by increasing the time interval between images
		Fluctuating environmental conditions	Ensure that the temperature and CO ₂ concentration are constant during imaging

● TIMING

Steps 1–9, production of lentivirus: 3 d. Assembly of the lentiviral solution and application to the cells (Steps 2–8) typically take 60 min, including incubation time. Cells require 48 h to produce lentivirus (Step 9).
Steps 10–13, harvest of lentivirus: ~1 h–1 d. Harvesting lentivirus from cells takes 20 min (Steps 10–12). An additional optional round of harvesting from the same cells requires 24 h of incubation (Step 13).
Step 14A, infection of target cells without spin treatment: 20 min
Step 14B, infection of cells with spin treatment: 90 min
Steps 15–19, selection of infected cells: 2–5 d. Replacing medium on cells takes 10 min (Step 15). Optional imaging of cells requires 3 h, including time to trypsinize and transfer cells (Step 16). Cells require incubation for 24–72 h (Step 17), depending on selection agent used, and 24–48 h (Steps 18 and 19) to recover. Dependent on the infection rate, this part of the protocol might require more time for cells to grow to sufficient confluency.
Steps 20–25, plating of cells for imaging: 13–28 h. Coating an optical-bottom 96-well plate with fibronectin for imaging requires 1–3 h (Steps 20–25). Counting cells and transferring to the imaging plate requires ~60 min (Step 26). Cells require 12–24 h to adhere and spread out before proceeding to subsequent steps.
Steps 26–31, live-cell imaging: 2–8 h: replacing medium on cells takes 10 min (Step 26). Optional Hoechst staining takes 20 min (Step 27). Setting up the microscope for imaging takes 30–60 min, depending on the number of cell lines and KTRs being imaged and the number of replicates (Step 28). Imaging takes 2–4 h (Steps 29–31).
Steps 32–39, data analysis: 1–5 d: the length of time required for data analysis (Steps 32–39) depends on the size and complexity of the imaging data. Typically, several hours of computational time will be required.

ANTICIPATED RESULTS

The imaging protocol will produce many images in a 16-bit TIF format. The total number of images can be calculated as: (number of KTRs + 1 for the nuclear marker) × (number of frames) × (number of positions).

Typically, KTR translocation can be rapidly observed upon addition of stimulants or inhibitors. The nuclear and cytoplasmic regions of each cell can then be segmented and tracked computationally to calculate the C/N ratio at a single-cell level (**Fig. 4**).

Importantly, the C/N ratio is related to—but not identical to—the concentration of the active kinase, because some time is required for the KTR kinase substrate to be phosphorylated by the active kinase and translocated to the cytoplasm. For example, when cells harboring the JNK KTR were treated with IL-1 β (to stimulate JNK activity), the peak C/N ratio was identified at 15 min (**Supplementary Fig. 2**; note that images were acquired at 2.5-min intervals). Subsequent analysis using our computational model estimated the peak in kinase activity to occur 10 min after stimulation. In other words, for the conditions of this experiment, kinase activation precedes KTR translocation by roughly 5 min. By the same reasoning, we expect that the decrease in the active kinase fraction precedes KTR dephosphorylation and re-translocation to the nucleus.

CellTK produces the output of each image processing step in a TIF format with a designated output directory. This includes images created after preprocessing, segmentation, tracking, and post-cleaning steps. CellTK parameters and usage may need to be optimized, depending on the cell type, cell density, nuclear marker, and/or other experimental factors. Note also that

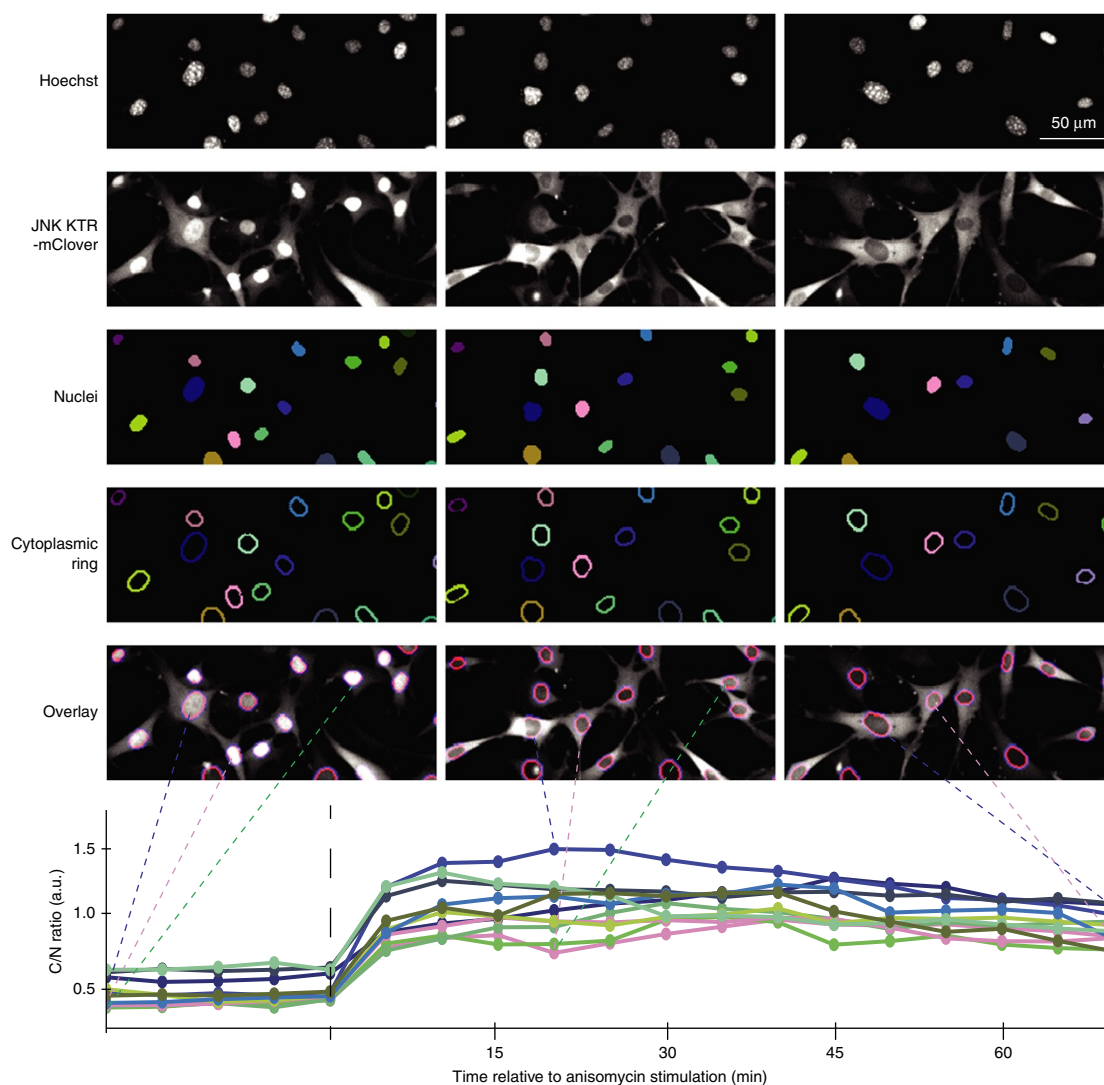


Figure 4 | Schematic outlining image and downstream analysis workflow. First, the nuclear region is segmented and tracked from the Hoechst-stained nuclear images. Next, the cytoplasmic ring is segmented by dilation from the nuclear region, followed by filtering based on KTR intensity. Finally, median pixel intensities of the nuclear region and cytoplasmic ring are extracted, and the cytoplasmic/nuclear intensity ratio is calculated at each time step, as a proxy for kinase activity dynamics.

the configuration files for the data sets provided for testing CellTK are optimized to reduce false-positive errors (for example, cells that do not appear in all frames are discarded). The final output of CellTK analysis is created as .csv or .npz files, both of which contain a list of single-cell properties over frames, such as cellular area and intensity statistics.

The C/N ratio is the quantitative measure of dynamic kinase activity extracted from the image stack, and is calculated by dividing cytoplasmic median intensity by nuclear median intensity. Further postcleaning of the extracted C/N ratio is generally recommended to deal with experimental, computational, and biological error. Although the C/N ratio normalizes for the KTR expression level across cells, it can be misleading in cases in which expression is so low that the corresponding fluorescence intensity approaches the background signal. In addition, nuclear or cytoplasmic regions can sometimes be mis-segmented if images of the nuclear marker are not clear or cells are too confluent. Likewise, cells may have many different morphologies or cell states (e.g., cell division or cell death) during imaging, and this inevitably leads to difficulties in measuring the C/N ratio quantitatively. In the **Supplementary Methods**, we describe how we implement the data cleaning of the extracted C/N ratio.

Note: Any Supplementary Information and Source Data files are available in the online version of the paper.

ACKNOWLEDGMENTS We thank the members of Covert lab for advice and critical commentary on the manuscript, in particular K. Lane for supplying the images of primary macrophages in **Supplementary Figure 1**. We gratefully acknowledge funding from several sources, including a Distinguished Investigator award and a Discovery Center grant from the Paul Allen Family Foundation, as well as an NIH Pioneer Award (5DP1LM01150-05) to M.W.C., a Human Frontier Science Program (HFSP) postdoctoral fellowship (LT000529/ 2012-L) to S.R., the Nakajima Foundation Scholarship to T.K., a DOE CSGF grant (DE-FG02-97ER25308) to D.N.M., and a Systems Biology Center grant (P50 GM107615).

AUTHOR CONTRIBUTIONS S.R. developed the reporter strategy and designed the experiments. T.K. and D.N.M. developed the computational pipelines and prepared the protocols. J.J.H. and S.A. developed the general workflow for the modeling. T.K., S.J., and M.W.C. wrote the manuscript, with input from all authors.

COMPETING FINANCIAL INTERESTS The authors declare no competing financial interests.

Reprints and permissions information is available online at <http://www.nature.com/reprints/index.html>. Publisher's note: Springer Nature remains neutral with regard to jurisdictional claims in published maps and institutional affiliations.

- Manning, G., Whyte, D.B., Martinez, R., Hunter, T. & Sudarsanam, S. The protein kinase complement of the human genome. *Science* **298**, 1912–1934 (2002).
- Cohen, P. & Philip, C. The role of protein phosphorylation in human health and disease. *Eur. J. Biochem.* **268**, 5001–5010 (2001).
- Purvis, J.E. & Lahav, G. Encoding and decoding cellular information through signaling dynamics. *Cell* **152**, 945–956 (2013).
- Selimkhanov, J. *et al.* Accurate information transmission through dynamic biochemical signaling networks. *Science* **346**, 1370–1373 (2014).
- Shalek, A.K. *et al.* Single-cell RNA-seq reveals dynamic paracrine control of cellular variation. *Nature* **510**, 363–369 (2014).
- Zernicka-Goetz, M., Morris, S.A. & Bruce, A.W. Making a firm decision: multifaceted regulation of cell fate in the early mouse embryo. *Nat. Rev. Genet.* **10**, 467–477 (2009).
- Vlamakis, H., Aguilar, C., Losick, R. & Kolter, R. Control of cell fate by the formation of an architecturally complex bacterial community. *Genes Dev.* **22**, 945–953 (2008).
- Spencer, S.L. *et al.* The proliferation-quiescence decision is controlled by a bifurcation in CDK2 activity at mitotic exit. *Cell* **155**, 369–383 (2013).
- Albeck, J.G., Mills, G.B. & Brugge, J.S. Frequency-modulated pulses of ERK activity transmit quantitative proliferation signals. *Mol. Cell* **49**, 249–261 (2013).
- Regot, S., Hughey, J.J., Bajar, B.T., Carrasco, S. & Covert, M.W. High-sensitivity measurements of multiple kinase activities in live single cells. *Cell* **157**, 1724–1734 (2014).
- Kondoh, K., Terasawa, K., Morimoto, H. & Nishida, E. Regulation of nuclear translocation of extracellular signal-regulated kinase 5 by active nuclear import and export mechanisms. *Mol. Cell. Biol.* **26**, 1679–1690 (2006).

- Nardozi, J.D., Lott, K. & Cingolani, G. Phosphorylation meets nuclear import: a review. *Cell Commun. Signal.* **8**, 32 (2010).
- Noursadeghi, M. *et al.* Quantitative imaging assay for NF- κ B nuclear translocation in primary human macrophages. *J. Immunol. Methods* **329**, 194–200 (2008).
- Maryu, G., Matsuda, M. & Aoki, K. Multiplexed fluorescence imaging of ERK and Akt activities and cell-cycle progression. *Cell Struct. Funct.* **41**, 81–92 (2016).
- Oldach, L. & Zhang, J. Genetically encoded fluorescent biosensors for live-cell visualization of protein phosphorylation. *Chem. Biol.* **21**, 186–197 (2014).
- Lam, A.J. *et al.* Improving FRET dynamic range with bright green and red fluorescent proteins. *Nat. Methods* **9**, 1005–1012 (2012).
- Kosugi, S., Hasebe, M., Tomita, M. & Yanagawa, H. Nuclear export signal consensus sequences defined using a localization-based yeast selection system. *Traffic* **9**, 2053–2062 (2008).
- Kosugi, S., Hasebe, M., Tomita, M. & Yanagawa, H. Systematic identification of cell cycle-dependent yeast nucleocytoplasmic shuttling proteins by prediction of composite motifs. *Proc. Natl. Acad. Sci. USA* **106**, 10171–10176 (2009).
- Sieracki, N.A. & Komarova, Y.A. Studying cell signal transduction with biomimetic point mutations. In *Manipulation of DNA and Protein – Examples from Current Research*, 381–392. (In Tech, 2013).
- Miyamoto, T. *et al.* Compartmentalized AMPK signaling illuminated by genetically encoded molecular sensors and actuators. *Cell Rep.* **11**, 657–670 (2015).
- Miura, H., Haruko, M., Michiyuki, M. & Kazuhiro, A. Development of a FRET biosensor with high specificity for Akt. *Cell Struct. Funct.* **39**, 9–20 (2014).
- Seong, J. *et al.* Detection of focal adhesion kinase activation at membrane microdomains by fluorescence resonance energy transfer. *Nat. Commun.* **2**, 406 (2011).
- Ubersax, J.A. & Ferrell, J.E. Jr. Mechanisms of specificity in protein phosphorylation. *Nat. Rev. Mol. Cell Biol.* **8**, 530–541 (2007).
- Pearce, L.R., Komander, D. & Alessi, D.R. The nuts and bolts of AGC protein kinases. *Nat. Rev. Mol. Cell Biol.* **11**, 9–22 (2010).
- Moritz, A. *et al.* Akt-RSK-S6 kinase signaling networks activated by oncogenic receptor tyrosine kinases. *Sci. Signal.* **3**, ra64 (2010).
- Hornbeck, P.V. *et al.* PhosphoSitePlus, 2014: mutations, PTMs and recalibrations. *Nucleic Acids Res.* **43**, D512–D520 (2015).
- McNulty, D.E., Sikorski, T.W. & Annan, R.S. Identification and analysis of protein phosphorylation by mass spectrometry. In *Analysis of Protein Post-Translational Modifications by Mass Spectrometry* 17–87 (2016).
- Peck, S.C. Analysis of protein phosphorylation: methods and strategies for studying kinases and substrates. *Plant J.* **45**, 512–522 (2006).
- Van Valen, D.A. *et al.* Deep learning automates the quantitative analysis of individual cells in live-cell imaging experiments. *PLoS Comput. Biol.* **12**, e1005177 (2016).
- Schindelin, J. *et al.* Fiji: an open-source platform for biological-image analysis. *Nat. Methods* **9**, 676–682 (2012).
- Carpenter, A.E. *et al.* CellProfiler: image analysis software for identifying and quantifying cell phenotypes. *Genome Biol.* **7**, R100 (2006).
- Edelstein, A.D. *et al.* Advanced methods of microscope control using μ Manager software. *J. Biol. Methods* **1**, e10 (2014).
- Magidson, V. & Khodjakov, A. Circumventing photodamage in live-cell microscopy. *Methods Cell Biol.* **114**, 545–560 (2013).

34. Basu, S., Campbell, H.M., Dittel, B.N. & Ray, A. Purification of specific cell population by fluorescence activated cell sorting (FACS). *J. Vis. Exp.* <http://dx.doi.org/10.3791/1546> (2010).
35. Masip, M.E. *et al.* Reversible cryo-arrest for imaging molecules in living cells at high spatial resolution. *Nat. Methods* **13**, 665–672 (2016).
36. Tay, S. *et al.* Single-cell NF-kappaB dynamics reveal digital activation and analogue information processing. *Nature* **466**, 267–271 (2010).
37. Williams, R.G. *et al.* Generation and characterization of a stable MK2-EGFP cell line and subsequent development of a high-content imaging assay on the Cellomics ArrayScan platform to screen for p38 mitogen-activated protein kinase inhibitors. *Methods Enzymol.* 364–389 (2006).
38. Anton, R. *et al.* A p38 substrate-specific MK2-EGFP translocation assay for identification and validation of new p38 inhibitors in living cells: a comprising alternative for acquisition of cellular p38 inhibition data. *PLoS ONE* **9**, e95641 (2014).
39. Reinhardt, H.C. *et al.* DNA damage activates a spatially distinct late cytoplasmic cell-cycle checkpoint network controlled by MK2-mediated RNA stabilization. *Mol. Cell* **40**, 34–49 (2010).
40. Samsonov, A. *et al.* Tagging of genomic STAT3 and STAT1 with fluorescent proteins and insertion of a luciferase reporter in the cyclin D1 gene provides a modified A549 cell line to screen for selective STAT3 inhibitors. *PLoS ONE* **8**, e68391 (2013).
41. Yissachar, N. *et al.* Dynamic response diversity of NFAT isoforms in individual living cells. *Mol. Cell* **49**, 322–330 (2013).
42. Gross, S.M. & Rotwein, P. Akt signaling dynamics in individual cells. *J. Cell Sci.* **128**, 2509–2519 (2015).
43. Katsura, Y. *et al.* An optogenetic system for interrogating the temporal dynamics of Akt. *Sci. Rep.* **5**, 14589 (2015).
44. Gross, S.M. & Peter, R. Mapping growth-factor-modulated Akt signaling dynamics. *Development* **143**, e1.2 (2016).
45. Schmierer, B. & Hill, C.S. Kinetic analysis of Smad nucleocytoplasmic shuttling reveals a mechanism for transforming growth factor-dependent nuclear accumulation of Smads. *Mol. Cell. Biol.* **25**, 9845–9858 (2005).
46. Wang, C.-C. *et al.* A time- and matrix-dependent TGFBR3–JUND–KRT5 regulatory circuit in single breast epithelial cells and basal-like premalignancies. *Nat. Cell Biol.* **16**, 345–356 (2014).
47. Hahn, A.T., Jones, J.T. & Meyer, T. Quantitative analysis of cell cycle phase durations and PC12 differentiation using fluorescent biosensors. *Cell Cycle* **8**, 1044–1052 (2009).
48. Zhao, B. *et al.* Inactivation of YAP oncoprotein by the Hippo pathway is involved in cell contact inhibition and tissue growth control. *Genes Dev.* **21**, 2747–2761 (2007).
49. Cohen-Saidon, C., Cohen, A.A., Sigal, A., Liron, Y. & Alon, U. Dynamics and variability of ERK2 response to EGF in individual living cells. *Mol. Cell* **36**, 885–893 (2009).